Available online at www.sciencedirect.com

ScienceDirect

www.elsevier.com/locate/jes

JES JOURNAL OF ENVIRONMENTAL SCIENCES

www.jesc.ac.cn

Emission of intermediate volatility organic compounds from a ship main engine burning heavy fuel oil

Haijun Lou[1], *Yuejiao Hao*[2,4], *Weiwei Zhang*[2,4], *Penghao Su*[2,4,*], *Fan Zhang*[3], *Yingjun Chen*[3], *Daolun Feng*[1,4], *Yifan Li*[5]

1. *College of Merchant Marine, Shanghai Maritime University, Shanghai 201306, China*
2. *Department of Environmental Engineering, Shanghai Maritime University, Shanghai 201306, China*
3. *College of Environmental Science and Engineering, Tongji University, Shanghai 200092, China*
4. *International Joint Research Center for Persistent Toxic Substances (IJRC-PTS), Shanghai Maritime University, Shanghai 200135, China*
5. *International Joint Research Center for Persistent Toxic Substances (IJRC-PTS-NA), Toronto, Ontario M2N 6X9, Canada*

ARTICLE INFO

Article history:
Received 5 December 2018
Revised 25 April 2019
Accepted 29 April 2019
Available online 8 May 2019

Keywords:
Marine main engine
Intermediate-volatility organic compounds
Heavy fuel oil
Emission factor
Chemical composition
Distribution

ABSTRACT

Intermediate volatility organic compounds (IVOCs) are crucial precursors of secondary organic aerosol (SOA). In this study, gaseous IVOCs emitted from a ship main engine burning heavy fuel oil (HFO) were investigated on a test bench, which could simulate the real-world operations and emissions of ocean-going ships. The chemical compositions, emission factors (EFs) and volatility distributions of IVOC emissions were investigated. The results showed that the main engine burning HFO emitted a large amount of IVOCs, with average IVOC EFs of 20.2–201 mg/kg-fuel. The IVOCs were mainly comprised of unspeciated compounds. The chemical compositions of exhaust IVOCs were different from that of HFO fuel, especially for polycyclic aromatic compounds and alkylcyclohexanes. The volatility distributions of IVOCs were also different between HFO exhausts and HFO fuel. The distinctions in IVOC emission characteristics between HFO exhausts and HFO fuel should be considered when assessing the IVOC emission and related SOA formation potentials from ocean-going ships burning HFO, especially when using fuel-surrogate models.

Introduction

Heavy fuel oil (HFO) is used as fuel for the main and auxiliary engines of ocean-going ships (Huang et al., 2018a; Puskar et al., 2018). Burning HFO can emit a large amount of harmful pollutants, such as black carbon, sulfur dioxide, nitrogen oxides and particulate matter (Huang et al., 2018b; Moldanová et al., 2013; Sippula et al., 2014; Zhang et al., 2016; Zhao et al., 2013). Although nearshore ships shift from HFO to distillate fuels to reduce emissions in accordance with the regulations of the International Maritime Organization (Sippula et al., 2014; Streibel et al., 2017), ocean-going ships use HFO as a routine fuel around the world. Because nearly 70% of ocean-going ships are sailing along routes within 400 km of coastlines, the exhaust can migrate to the coastal areas under adverse weather conditions (Eyring et al., 2010, 2005). Around the world, about 60,000 people die annually from diseases such as cardiovascular disease and lung cancer caused by pollutants emitted by ocean-going ships (Kulmala, 2015).

* *Corresponding author. E-mail:* phsu@shmtu.edu.cn (Penghao Su).

https://doi.org/10.1016/j.jes.2019.04.029
1001-0742 © 2019 The Research Center for Eco-Environmental Sciences, Chinese Academy of Sciences. Published by Elsevier B.V.

In addition, ships burning HFO can emit large amounts of organic compounds (Huang et al., 2018a). Among the exhaust organic compounds, intermediate volatility organic compounds (IVOCs), with the effective saturation concentration (C^*) of 10^3–10^6 μg/m^3, are found to be crucial precursors of secondary organic aerosol (SOA) (Ait-Helal et al., 2014; Gentner et al., 2017; Hayes et al., 2015; Ots et al., 2016; Robinson et al., 2007; Zhao et al., 2014, 2015, 2016). SOA is of concern to researchers due to its great proportion and hazard in fine particles (Couvidat et al., 2018; Hallquist et al., 2009; Hui et al., 2019), which can penetrate into the lungs and cardiovascular system and cause heart and lung cancer deaths (Huck et al., 2017; Kim et al., 2017; Liu et al., 2017; Manojkumar et al., 2019). Thus, understanding IVOC emissions and corresponding SOA potentials from ships burning HFO is helpful in assessing the effects of ocean-going ship exhaust on coastal air quantity comprehensively.

To our knowledge, very limited studies have been conducted on the IVOC emissions from ships burning HFO until now (Huang et al., 2018a; Pieber et al., 2016), and the IVOC emission characteristics have not yet been revealed comprehensively. Therefore, in this study, emission factors, chemical compositions and volatility distributions of IVOCs emitted from a typical ship main engine burning HFO under various loads are investigated, and compared with those of HFO fuel, to further understand the IVOC emission characteristics and corresponding SOA potentials.

1. Materials and methods

1.1. Test fuels, engine and operation modes

A 100-hr test was conducted on the MAN 6S35ME-B9 marine two-stroke low-speed engine in the Engine Performance Test Laboratory of Shanghai Maritime University, which has been widely used as the main engine on board. The test bench is equipped with a hydraulic dynamometer, and can simulate the real-world operations and emissions of ocean-going ships. The detailed fuel properties of HFO are as follows: flash point 81°C, density at 20°C 976 kg/m^3, viscosity at 50°C 160.8 mm^2/sec, sulfur content 2.13% (W/W), water content 0.32% (V/V), and pour point 13.5°C. Moreover, the following are engine specifications information: compression ratio 21, bore/stroke 550/1550 (mm/mm), rated speed 142 r/min, rated power 3570 kW, ignition order 1–5–3–4–2–6, and intake type inter-cooling. The deposited carbons were cleaned from the nozzle and cylinder and the piston rings were renewed before testing.

1.2. Sampling methods and exhaust measurements

Samplings were performed when the cooling water temperature, the lubricating oil temperature and the exhaust temperature had reached a steady state. Three parallel samples were collected for each load.

Before sampling, the exhaust was diluted with ambient air at a ratio of ~10:1. Thereafter, the exhaust was drawn through a quartz filter followed by two tandem stainless steel tubes filled with Tenax TA (SEFM-S60 Agilent, Agilent Technologies, USA) filled with ~200 mg of Tenax TA for each tube at a flow rate of 0.4 L/min to collect IVOCs. Samples were deemed to be valid when the IVOC mass in the downstream tube was less than 10% of that in the upstream tube. The quartz filters were baked at 450°C for 6 hr and the Tenax tubes were baked at 300°C under a nitrogen stream for 2 hr before sampling. Blank tubes were also incorporated for analyses and were handled and processed in an identical manner as the sample tubes. Fuel consumption and CO_2 concentrations were continuously measured during samplings. The dilution and measurement methods are described in our previous study (Su et al., 2018).

1.3. IVOCs analysis

Known amounts of deuterated standards (d_8-naphthalene and d_{10}-acenaphthene, d_{10}-phenanthrene, C_{16}, C_{20}, C_{24} deuterated *n*-alkanes where "*n*" was the carbon number of straight-chain alkanes) were injected into each Tenax tube prior to thermal desorption to determine the recovery of IVOCs during analysis. The Tenax samples were analyzed using an gas chromatograph (Agilent 7890-5975C, Agilent Technologies, USA) coupled with a mass-selective detector (GC/MSD), equipped with a DB-5 capillary column (30 m, 0.25 mm id, 0.25 μm film thickness, Agilent, USA) and a thermal desorption sample extraction and injection system (Optic4, GL Sciences B.V., Japan). IVOCs were thermally desorbed from the tube in splitless flow mode with a helium flow of 50 mL/min, via a temperature program of 30 to 275°C at a rate of 60°C/min and hold for 5 min. Thereafter, desorbed IVOCs were enriched by a cold trap at −120°C. The enriched IVOCs were thermally desorbed in a split flow mode with a helium flow of 20 mL/min and a split ratio of 7.7:1, via a temperature program of −120 to 300°C at a rate of 60°C/min and hold for 5 min. Finally, IVOCs were determined using GC/MSD. Helium was used as the carrier gas at a constant flow of 0.5 mL/min. The temperatures of the transfer line and EI (electron impact ionization) source were 310 and 230°C, respectively. The column oven temperature program was: 6°C/min from 60 to 300°C and hold for 8 min.

For HFO fuel, 10 μL of HFO was spiked with a known amount of deuterated standards and extracted with 20 mL of dichloromethane for 20 min in an ultrasonic bath. The extracts were reduced to 2 mL under a gentle stream of nitrogen and cleaned up using dispersive solid phase extraction (SPE, Agilent Part No. 5982-5421, Agilent Technologies, USA). After centrifugation for 5 min at 2500 r/min, the supernatant was solvent-exchanged into isooctane to a final volume of 1 mL. A known amount of volumetric internal standard (hexamethylbenzene) was added prior to instrumental analysis. The mass spectral analysis of IVOCs in HFO was the same as described above.

1.4. Quantification of IVOCs and emission factor

The quantification method of IVOCs in this study was performed according to previously reported methods (Huang et al., 2018a; Zhao et al., 2014). Briefly, IVOCs were identified by matching the mass spectra obtained with the mass spectra from the standards and National Institute of Standards and Technology (NIST) library (https://webbook.nist.gov/chemistry/name-ser/). IVOCs were classified into straight-chain alkanes (*n*-alkanes) and branched alkanes (b-alkanes), cycloalkanes, alkylcyclohexanes,

Table 1 – Engine test cycle and fuel consumption.

Time (min)	Engine load	Engine speed (r/min)	Fuel consumption rate (g/kWh)
30	25%	90	220
30	50%	114	200
500	75%	130	192
10	90%	130	190

unsubstituted and substituted polycyclic aromatic hydrocarbons (PAHs), single-ring aromatics and unspeciated cyclic compounds. The total ion signal was integrated into 11 bins (B_n) based on the GC retention times of *n*-alkanes. Emissions of individual IVOCs were quantified based on the calibrated instrument response to authentic standards and accounting for recovery of the deuterated internal standard. Naphthalene (nap), 1-methylnaphthalene, 2-methylnaphthalene (C1-Nap), 1,2-dimethylnaphthalene (C2-Nap), acenaphthylene (Acp), acenaphthene (Ace), fluorene (Flu), phenanthrene (Phe), anthracene (Ant), fluoranthene (Fluo), pyrene (Pyr), *n*-alkanes and deuterated standards were used as authentic standards. The recoveries of the deuterated internal standards were 71.3%–114%.

The exhaust flow rates for the engine were calculated using the carbon balance method specified in ISO 8178-2, assuming complete conversion of fuel carbon to CO_2 (Corrêa and Arbilla, 2006). Based on the fuel consumption (Table 1) and the concentrations of IVOCs, the emission factors (EFs) of gaseous phase IVOCs were determined.

2. Results and discussion

2.1. Chemical composition of IVOCs

The chemical characteristics of the IVOCs were illustrated by the average mass spectrum of the total IVOCs (in B_{12}-B_{22}). Fig. 1a–d shows the average mass spectrum of IVOCs in the exhausts from the engine fueled with HFO collected under four loads.

The IVOC mass spectra exhibited that the chemical composition varied for different loads. The primary mass fragment was mass-to-charge ratio (*m*/*z*) of 128 for loads of 25% and 50%, while the *m*/*z* of 57 was dominant in mass fragments of loads of 75% and 90%. The *m*/*z* 57 and 128 peaks are the main mass fragments of alkanes and naphthalene (Dall'Osto et al., 2012), respectively. In addition, cycloalkanes (*m*/*z* 55, 69 and 97), alkylcyclohexane (*m*/*z* 83) (Moldanová et al., 2009; Zhao et al., 2014; https://webbook.nist.gov/chemistry/name-ser/), single-ring aromatic hydrocarbons (*m*/*z* 91 and 105) (Gentner et al., 2012) and substituted

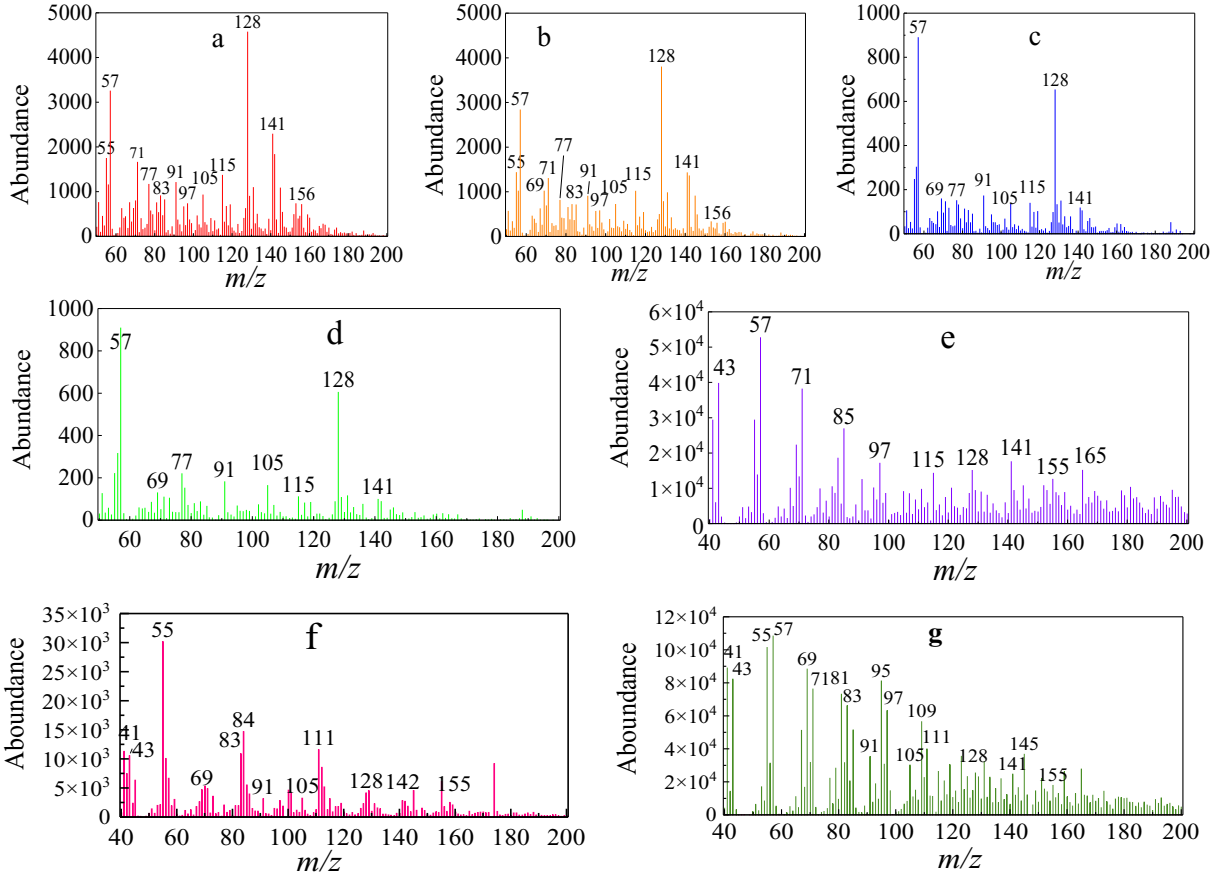

Fig. 1 – Average mass spectra of heavy fuel oil (HFO) exhausts at (a) 25%, (b) 50%, (c) 75%, and (d) 90% engine loads and (e) HFO fuel, and average mass spectra of marine gas oil (MGO) exhaust at (f) 75% load and (g) MGO fuel. *m*/*z*: mass-to-charge ratio.

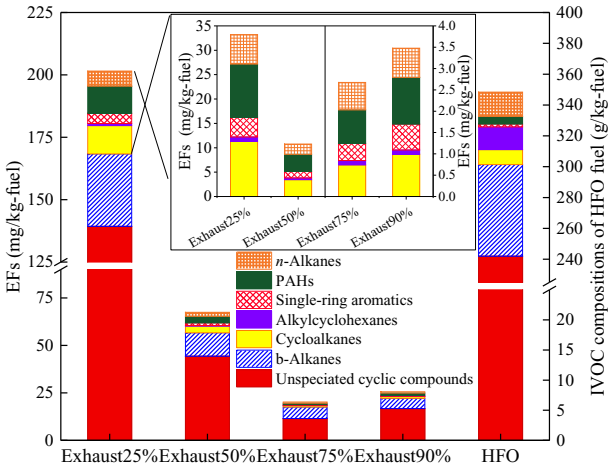

Fig. 2 – Emission factors (EFs) of exhaust at 25% (Exhaust25%), 50% (Exhaust50%), 75% (Exhaust75%), and 90% (Exhaust90%) engine loads and the intermediate volatility organic compounds (IVOCs) of HFO fuel. Inset: a magnified view of the emission factors for straight-chain alkanes (*n*-alkanes), polycyclic aromatic hydrocarbons (PAHs), single-ring aromatics, alkylcyclohexanes and cycloalkanes in HFO fuel and exhausts from four engine loads. b-alkanes: branched alkanes.

naphthalene (*m*/*z* 141) were also major contributors to IVOCs. The mass fragments of aliphatic hydrocarbons (*m*/*z* 43, 55, 57, 69, 71, 83 and 111) in the exhausts were more abundant than those of the aromatic compounds (*m*/*z* 91, 105, 128, 141, 155).

In addition, as shown in Fig. 1e, the average mass spectrum of HFO fuel was mainly composed of *n*- and b-alkanes (*m*/*z* 43, 57, 71 and 85), and also included cycloalkanes (*m*/*z* 97) and aromatic compounds (*m*/*z* 128, 141 and 155). The difference between the mass spectra of HFO exhaust and HFO fuel was observed mainly in the proportions of naphthalene (*m*/*z* 128).

For comparison, the average mass spectra of IVOCs emitted from marine gas oil (MGO), which represents a common alternative nearshore fuel, are also shown in Fig. 1f–g. The tests of MGO were conducted on an auxiliary engine and the results will be reported in our other paper. A primary comparison was conducted between HFO and MGO herein due the difference in test engines. Fig. 1 illustrates that HFO and MGO fuel exhibited similar chemical compositions, whereas HFO exhaust contained greater portions of naphthalene (*m*/*z* 128) and substituted naphthalene (*m*/*z* 141) as compared to MGO exhaust.

Compared with the IVOC emissions of vehicles, the IVOC composition of HFO exhausts in this study was similar to that of diesel vehicle exhaust, which is also dominated by aliphatic compounds (*m*/*z* 43, 57 and 71) (Zhao et al., 2015). In contrast, gasoline vehicle exhaust contains more aromatic components (*m*/*z* 91, 105, 128, 141 and 156) (Zhao et al., 2016).

2.2. Emission factor

The emission factors (EFs) of detected IVOCs (in chemical classes) were calculated and are shown in Fig. 2. The total IVOC mass (ΣIVOC) EFs of the HFO exhausts under the loads of 25%, 50%, 75% and 90% were 201 ± 13.1, 67.5 ± 19.7, 20.2 ± 6.43 and 25.6 ± 10.8 mg/kg-fuel, respectively. The smallest EFs were observed at the 75% load, which were as low as ~10% and ~30% of the EFs at 25% and 50% loads, respectively. With respect to 90% load, the EFs were higher than that of the 75% load. This was speculated to be related to the difference in air-fuel ratio between 75% and 90% loads. The engine was operated by increasing air intake under constant engine speed to increase the load after 75% load (Table 1). Thus, the combustion at 90% load took place under a higher air–fuel ratio and a correspondingly lower combustion temperature as compared to 75% load. And, the lower combustion temperature at 90% load led to an increase in IVOC emissions. By comparison, ΣIVOC EFs in the MGO-fueled auxiliary engine exhausts under the loads of 25%, 50%, 75% were 93.8 ± 0.1, 50.9 ± 9.29, 2.33 ± 0.34 mg/kg-fuel, respectively.

Unspeciated cyclic compounds were the dominant contributors of IVOC emissions at all loads, accounting for over 57% of the ΣIVOCs (Fig. 3), followed by b-alkanes, accounting for about 15% of the ΣIVOCs (Fig. 3). These chemical

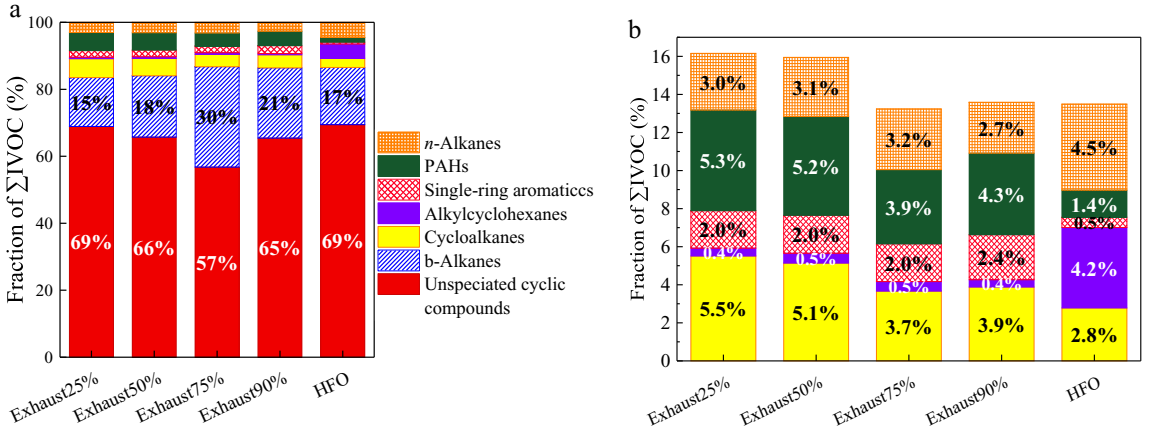

Fig. 3 – (a) Fractions of all IVOC compositions in the total IVOC compositions (ΣIVOCs) and (b) fractions of PAHs, single-ring aromatics, alkylcyclohexanes and cycloalkanes in the ΣIVOCs.

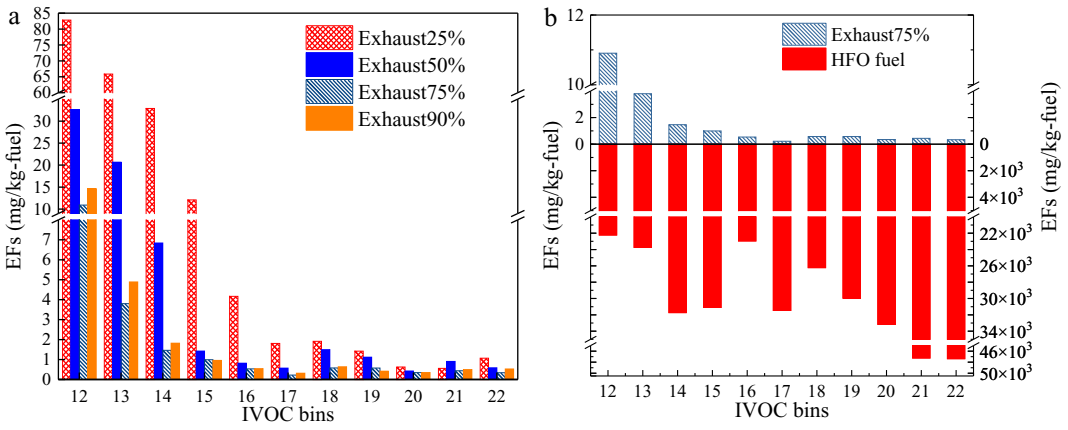

Fig. 4 – Comparison of the IVOC volatility distribution of the exhausts (a) at all loads and (b) at 75% load and IVOC composition of HFO fuel.

compositions were similar to those of MGO-fueled auxiliary engine exhaust, in which the fraction of unspeciated cyclic compounds and b-alkanes was 80% and 15%, respectively.

In addition, Fig. 3 also illustrates that HFO fuel contained IVOC compounds. This implied IVOC emissions when HFO fuel was emitted unburned. On ocean-going ships, unburned HFO fuel can arise from fuel preheating and non-ideal combustion. IVOCs in HFO fuel were comprised of similar fractions of unspeciated cyclic compounds and b-alkanes to those in HFO exhaust, while the fractions of other IVOC compounds in HFO exhausts varied from those in HFO fuel (Figs. 2 and 3). Compared with HFO fuel, the fraction of alkylcyclohexanes in HFO exhausts decreased significantly, while the fraction of PAHs in the exhausts increased. The variations in IVOC composition between HFO exhausts and HFO fuel implied that, for HFO, the IVOC emission characteristics were not likely correlated to the IVOC composition of the fuel.

2.3. Volatility distribution of IVOC EFs

The SOA formation potentials of IVOCs are dependent on the volatility distribution of IVOCs. In this study, the volatility distribution of IVOCs was studied using the IVOC bins (B_n). Fig. 4a shows that exhaust IVOCs exhibited similar volatility characteristics under different loads. Nevertheless, the volatility distributions of HFO exhaust IVOCs were different from those of HFO fuel (Fig. 4b). For HFO fuel, the IVOCs mainly distributed in the lower volatility bins (B_{21}–B_{22}), accounting for 30% of the total emissions. However, in exhausts, IVOCs mainly concentrated in the higher volatility range (B_{12}-B_{15}), with about half of the emissions in the B_{12} bin (Fig. 5).

With respect to individual classes of IVOCs, most detected compounds mainly distributed in higher volatility bins (B_{12}–B_{15}) at all loads (Fig. 6). The volatility distributions of individual classes of IVOCs in exhausts were significantly different from that of HFO fuel. For HFO fuel, large amounts of *n*-alkanes, b-alkanes, alkylcyclohexanes and unspeciated cyclic compounds distributed in the lower volatility bins (B_{19}–B_{22}), while in the exhausts these compounds mainly distributed in the higher volatility bins. In addition, cycloalkane and alkylcyclohexanes could be detected in every bin for HFO fuel, whereas they could be detected in the higher volatility bins (B_{12}–B_{16}) in the exhausts. Generally, compared with HFO fuel, exhaust IVOCs tended to distribute in higher volatility bins, except for IVOC PAHs, which distributed in higher volatility bins for both HFO fuel and exhausts. It was likely that the lower volatility IVOCs (B_{17}–B_{22}) in HFO fuel were prone to be combusted or transformed via pyrolysis processes (Tree and Svensson, 2007), and thus the IVOCs with higher volatility (B_{12}–B_{16}) were emitted as a result of incomplete combustion and pyrolysis processes. In contrast, the exhaust hydrocarbon compositions (including IVOCs) of volatile fuels (such as gasoline and diesel) likely depend more closely on the hydrocarbon compositions of the fuels, which is attributed to the emission of unburned fuels (Gentner et al., 2012).

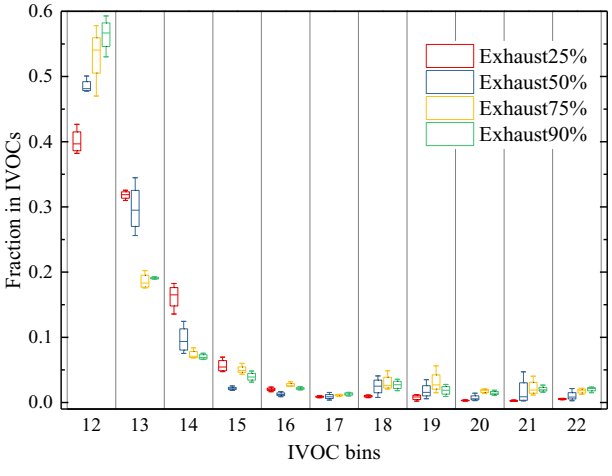

Fig. 5 – Box-whisker plot of mass fraction of IVOCs in each retention-time bin. The boxes represent the 75th and 25th percentiles with the centerline being the median. The whiskers are the 90th and 10th percentiles.

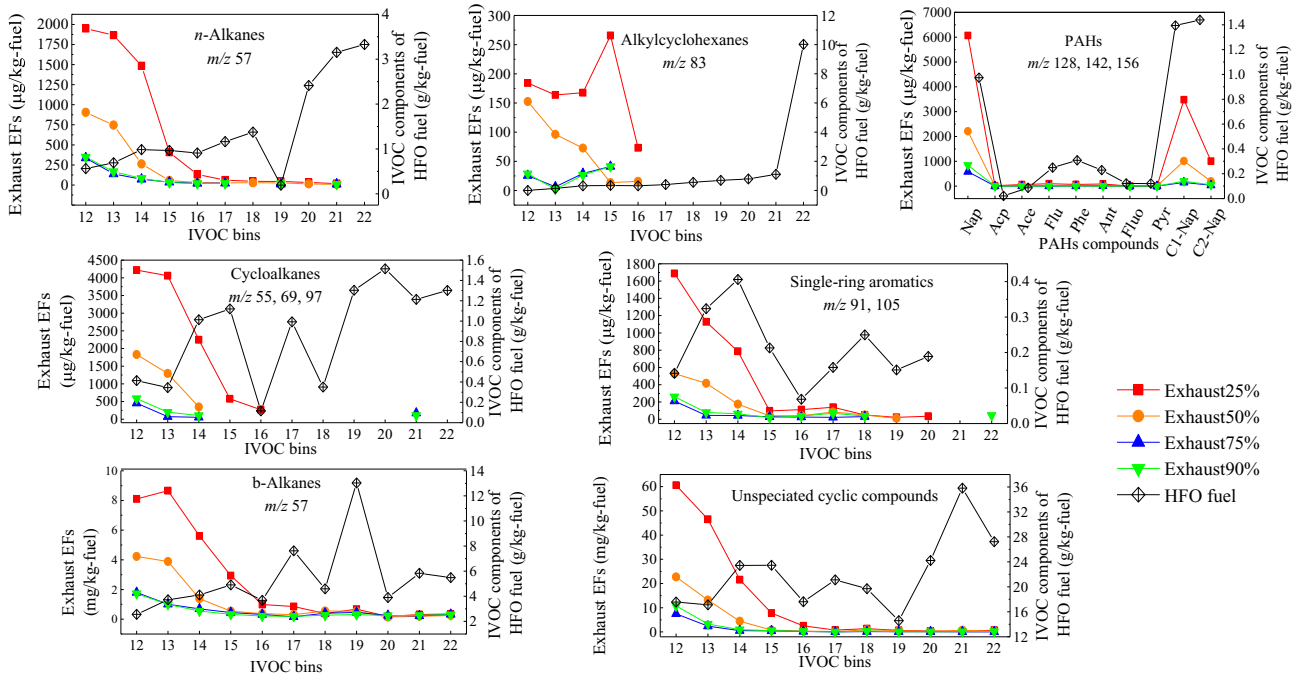

Fig. 6 – Volatility distributions of individual classes of IVOCs in exhausts and HFO fuel. Nap: naphthalene; Acp: acenaphthylene; Ace: acenaphthene; Flu: fluorene; Phe: phenanthrene; Ant: anthracene; Fluo: fluoranthene; Pyr: pyrene; C1-Nap: 1-methylnaphthalene, 2-methylnaphthalene; C2-Nap: 1,2-dimethylnaphthalene.

Fig. 6 also shows that the emissions of IVOCs with higher volatility (B_{12}–B_{15}) declined as the load increased from 25% to 75%. This could be attributed to the occurrence of complete combustion at higher loads, because the IVOCs with higher volatility were emitted via incomplete combustion, as discussed above.

It is noteworthy that, compared to the test bench exhaust results, the exhaust IVOCs of a real-world ocean-going ship's main engine burning the same HFO are comprised of more compounds in lower volatility bins (Huang et al., 2018a), and have more similarity to the IVOC components of HFO fuel (Fig. 4b). Thus, we speculated that the exhausts sampled from this real-world ocean-going ship contain more unburned HFO fuel, which may result from the deterioration of the engine after long-term navigation. In contrast, the engine tested in this study had undergone maintenance, including the cleaning of deposited carbons from the nozzle and cylinder and renewal of the piston rings, and thus the combustion likely took place under very good conditions. The optimized engine conditions during the test in this study likely mitigated the emissions of unburned fuels. The mitigation of unburned fuel emissions also resulted in lower IVOC EFs in this study, which were on the order of ~10^{-1} the magnitude of IVOC EFs in the literature, because even a small amount of fuel evaporation can dramatically impact IVOC emissions, as discussed in Section 2.2.

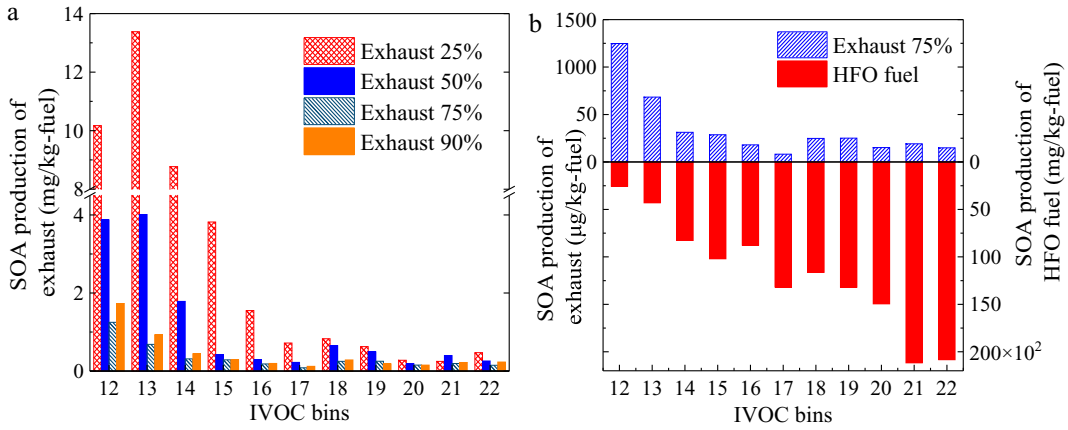

Fig. 7 – Secondary organic aerosol (SOA) production (a) at all loads and (b) at 75% load and SOA production of HFO fuel.

2.4. SOA production

The SOA production was calculated using a method described in the literature (Zhao et al., 2015) and shown in Fig. 7. The SOA production of the HFO exhausts under the loads of 25%, 50%, 75% and 90% was 40.9 ± 11.4, 12.6 ± 4.22, 3.79 ± 1.42 and 4.78 ± 1.70 mg/kg-fuel, respectively. Consistent with the case for IVOC EFs, exhaust IVOCs exhibited the smallest SOA production at 75% load (Fig. 7a). The SOA production of exhausts was mostly contributed by IVOC compounds in higher volatility bins at all loads (Fig. 7a). In contrast, the SOA production of HFO fuel (if unburned HFO fuel was released) was mainly contributed by the IVOC compounds in lower volatility bins (Fig. 7b). Considering that IVOC compounds with lower volatility exhibit greater SOA formation potential as compared to compounds with higher volatility in the same chemical class (Atkinson and Arey, 2003; Chan et al., 2009; Kwok and Atkinson, 1995; Zhao et al., 2014), the IVOC distributions in the higher volatility bins of HFO exhausts versus in the lower volatility bins of HFO fuel in this study suggested that reducing the unburned HFO fuel released due to non-ideal combustion via fuel preheating might be a more efficient method to mitigate the SOA production from IVOCs emitted by ocean-going ships burning HFO.

The change in the SOA production between HFO exhaust and HFO fuel should be noted (Fig. 7a). These distinctions indicated that one of the most widely used SOA assessment methods, i.e., the "Bottom-Up" method, which considers SOA formation potential using unburned (gasoline and diesel) fuels as emission surrogates on the basis of the compositional consistency between gasoline and diesel fuels and their exhausts (Gentner et al., 2017), should be applied to IVOC emissions from HFO with more caution.

3. Conclusions

(1) The HFO-fueled ship main engine emitted a large amount of IVOCs, and the average ΣIVOC EFs under four loads ranged from 20.2 to 201 mg/kg-fuel, which were much higher than those of the MGO-fueled marine auxiliary engine.
(2) The IVOC emissions were related to the engine load, and exhibited the smallest EFs at the load of 75%.
(3) The chemical compositions of IVOCs were different between HFO exhausts and HFO fuel. The HFO exhausts contained a greater proportion of PAHs, while the fraction of alkylcyclohexanes decreased significantly compared to HFO fuel.
(4) The volatility distributions of IVOCs were also different between HFO exhausts and HFO fuel. The IVOCs in exhausts were mainly concentrated in the higher volatility bins (B_{12}–B_{15}), while those of HFO fuel were mainly distributed in the lower volatility bins (B_{21}–B_{22}).
(5) The distinctions in IVOC emission characteristics between HFO exhausts and HFO fuel should be considered when assessing the IVOC emission and related SOA formation potentials from ocean-going ships burning HFO, especially when using fuel-surrogate models.

Acknowledgments

This study was financially supported by the National Natural Science Foundation of China (Nos. 41403084 and 4171101108), and the Project from Shanghai Committee of Science and Technology (No. 16ZR1414800).

REFERENCES

Ait-Helal, W., Borbon, A., Sauvage, S., Gouw, J.A., Colomb, A., Gros, V., et al., 2014. Volatile and intermediate volatility organic compounds in suburban Paris: variability, origin and importance for SOA formation. Atmos. Chem. Phys. 14, 10439–10464.
Atkinson, R., Arey, J., 2003. Atmospheric degradation of volatile organic compounds. Chem. Rev. 103, 4605–4638.
Chan, A.W.H., Kautzman, K.E., Chhabra, P.S., Surratt, J.D., Chan, A.W., Crounse, J.D., et al., 2009. Secondary organic aerosol formation from photooxidation of naphthalene and alkylnaphthalenes: implications for oxidation of intermediate volatility organic compounds (IVOCs). Atmos. Chem. Phys. 9, 3049–3060.
Corrêa, S.M., Arbilla, G., 2006. Aromatic hydrocarbons emissions in diesel and biodiesel exhaust. Atmos. Environ. 40, 6821–6826.
Couvidat, F., Vivanco, M.G., Bessagne, T.B., 2018. Simulating secondary organic aerosol from anthropogenic and biogenic precursors: comparison to outdoor chamber experiments, effect of oligomerization on SOA formation and reactive uptake of aldehydes. Atmos. Chem. Phys. 18, 15743–15766.
Dall'Osto, M., Ceburnis, D., Monahan, C., Worsnop, D.R., Bialek, J., Kulmala, M., et al., 2012. Nitrogenated and aliphatic organic vapors as possible drivers for marine secondary organic aerosol growth. J. Geophys. Res. Atmos. 117, 428–437.
Eyring, V., Köhler, H.W., Aardenne, J.V., Laue, A., 2005. Emissions from international shipping: 1. The last 50 years. J. Geophys. Res. 110, D17305.
Eyring, V., Isaksen, I.S.A., Berntsen, T., Collins, W.J., Corbett, J.J., Endresen, O., et al., 2010. Transport impacts on atmosphere and climate: shipping. Atmos. Environ. 44, 4735–4771.
Gentner, D.R., Isaacman, G., Worton, D.R., Chan, A.W.H., Dallmann, T.R., Davisa, L., et al., 2012. Elucidating secondary organic aerosol from diesel and gasoline vehicles through detailed characterization of organic carbon emissions. Proc. Natl. Acad. Sci. U. S. A. 109, 18318–18323.
Gentner, D.R., Jathar, S.H., Gordon, T.D., Bahreini, R., Day, D.A., El Haddad, I., et al., 2017. Review of urban secondary organic aerosol formation from gasoline and diesel motor vehicle emissions. Environ. Sci. Technol. 51, 1074–1093.
Hallquist, M., Wenger, J.C., Baltensperger, U., Rudich, Y., Simpson, D., Claeys, M., et al., 2009. The formation, properties and impact of secondary organic aerosol: current and emerging issues. Atmos. Chem. Phys. 9, 5155–5236.
Hayes, P.L., Carlton, A.G., Baker, K.R., Ahmadov, R., Washenfelder, R.A., Alvarez, S., et al., 2015. Modeling the formation and aging of secondary organic aerosols in Los Angeles during CalNex 2010. Atmos. Chem. Phys. 15, 5773–5801.
Huang, C., Hu, Q., Li, Y., Tian, J., Ma, Y., Zhao, Y., et al., 2018a. Intermediate volatility organic compound emissions from a large cargo vessel operated under real-world conditions. Environ. Sci. Technol. 52, 12934–12942.
Huang, C., Hu, Q., Wang, H., Qiao, L., Jing, S., Wang, H., et al., 2018b. Emission factors of particulate and gaseous compounds from a large cargo vessel operated under real-world conditions. Environ. Pollut. 242, 667–674.
Huck, J.J., Whyatt, J.D., Coulton, P., Davison, B., Gradinar, A., 2017. Combining physiological, environmental and locational

sensors for citizen-oriented health applications. Environ. Monit. Assess. 189, 114.
Hui, L., Liu, X., Tan, Q., Feng, M., An, J., Qu, Y., et al., 2019. VOC characteristics, sources and contributions to SOA formation during haze events in Wuhan, Central China. Sci. Total. Environ. 650, 2624–2639.
Kim, H.J., Choi, M.G., Park, M.K., Seo, Y.R., 2017. Predictive and prognostic biomarkers of respiratory diseases due to particulate matter exposure. J. Cancer Prev. 22, 6–15.
Kulmala, M., 2015. Atmospheric chemistry: China's choking cocktail. Nature 526, 497–499.
Kwok, E.S.C., Atkinson, R., 1995. Estimation of hydroxyl radical reaction rate constants for gas-phase organic compounds using a structure-reactivity relationship: An update. Atmos. Environ. 29, 1685–1695.
Liu, M., Huang, Y., Jin, Z., Ma, Z., Liu, X., Zhang, B., et al., 2017. The nexus between urbanization and PM2. 5 related mortality in China. Environ. Pollut. 227, 15–23.
Manojkumar, N., Srimuruganandam, B., Nagendra, S.M.S., 2019. Application of multiple-path particle dosimetry model for quantifying age specified deposition of particulate matter in human airway. Ecotoxicol. Environ. Safe. 168, 241–248.
Moldanová, J., Fridell, E., Popovicheva, O., Demirdjian, B., Tishkova, V., Faccinetto, A., et al., 2009. Characterisation of particulate matter and gaseous emissions from a large ship diesel engine. Atmos. Environ. 43, 2632–2641.
Moldanová, J., Fridell, E., Winnes, H., Holmin-Fridell, S., Boman, J., Jedynska, A., et al., 2013. Physical and chemical characterisation of PM emissions from two ships operating in European emission control areas. Atmos. Meas. Tech. 6, 3577–3596.
Ots, R., Young, D.E., Vieno, M., Xu, L., Dunmore, R.E., Allan, J.D., et al., 2016. Simulating secondary organic aerosol from missing diesel-related intermediate-volatility organic compound emissions during the Clean Air for London (ClearfLo) campaign. Atmos. Chem. Phys. 16, 6453–6473.
Pieber, S.M., Zhao, Y., Orasche, J., Stengel, B., Czech, H., Corbin, J.C., et al., 2016. Characterization of organic low-, semi-, intermediate- and volatile organic compounds from four-stroke ship engine emissions: implications for atmospheric processing. 22nd European Aerosol Conference. Tours, France. Sep 4–9.
Puskar, M., Kopas, M., Puskar, D., Lumnitzer, J., 2018. Method for reduction of the NOx emissions in marine auxiliary diesel engine using the fuel mixtures containing biodiesel using HCCI combustion. Mar. Pollut. Bull. 127, 752–760.
Robinson, A.L., Donahue, N.M., Shrivastava, M.K., Weitkamp, E.A., Sage, A.M., Grieshop, A.P., et al., 2007. Rethinking organic aerosols: semivolatile emissions and photochemical aging. Science 315, 1259–1262.
Sippula, O., Stengel, B., Sklorz, M., Streibel, T., Rabe, R., Orasche, J., et al., 2014. Particle emissions from a marine engine: chemical composition and aromatic emission profiles under various operating conditions. Environ. Sci. Technol. 48, 11721–11729.
Streibel, T., Schnelle-Kreis, J., Czech, H., Harndorf, H., Jakobi, G., Jokiniemi, J., et al., 2017. Aerosol emissions of a ship diesel engine operated with diesel fuel or heavy fuel oil. Environ. Sci. Pollut. Res. 24, 10976–10991.
Su, P., Geng, P., Wei, L., Hou, C., Yin, F., Tomy, G.T., et al., 2018. PM and PAHs emissions of ship auxiliary engine fuelled with waste cooking oil biodiesel and marine gas oil. IET Intell. Transp. Sy. 13, 218–227.
Tree, D.R., Svensson, K.I., 2007. Soot processes in compression ignition engines. Prog. Energ. Combust. 33, 272–309.
Zhang, F., Chen, Y., Tian, C., Lou, D., Li, J., Zhang, G., et al., 2016. Emission factors for gaseous and particulate pollutants from offshore diesel engine vessels in China. Atmos. Chem. Phys. 16, 6319–6334.
Zhao, M., Zhang, Y., Ma, W., Fu, Q., Yang, X., Li, C., et al., 2013. Characteristics and ship traffic source identification of air pollutants in China's largest port. Atmos. Environ. 64, 277–286.
Zhao, Y., Hennigan, C.J., May, A.A., Tkacik, D.S., de Gouw, J.A., Gilman, J.B., et al., 2014. Intermediate-volatility organic compounds: a large source of secondary organic aerosol. Environ. Sci. Technol. 48, 13743–13750.
Zhao, Y., Nguyen, N.T., Presto, A.A., Hennigan, C.J., May, A.A., Robinson, A.L., 2015. Intermediate volatility organic compound emissions from on-road diesel vehicles: chemical composition, emission factors, and estimated secondary organic aerosol production. Environ. Sci. Technol. 49, 11516–11526.
Zhao, Y., Nguyen, N.T., Presto, A.A., Hennigan, C.J., May, A.A., Robinson, A.L., 2016. Intermediate volatility organic compound emissions from on-road gasoline vehicles and small off-road gasoline engines. Environ. Sci. Technol. 50, 4554–4563.